Journal of Marine Research, 58, 755–778, 2000

Abyssal upwelling in the Indian Ocean: Radiocarbon diagnostics

by Ashwanth Srinivasan[1], Claes G. H. Rooth[1], Zafer Top[1] and D. B. Olson[1]

ABSTRACT

The GEOSECS Indian Ocean radiocarbon and carbonate chemistry data set are used to estimate the mean upwelling transport of bottom water in the Indian Ocean north of 30S. The study uses an ''adjusted radiocarbon concentration" which is corrected for the effects of addition of particulate radiocarbon to the deep ocean. The cross-basin uniformity in the vertical gradients of ''adjusted radiocarbon" allows quantification of vertical transfer processes using horizontally averaged concentration and fluxes. The estimated total upwelling flux, north of 30S, is $8.2 \pm 1.5 \times 10^6$ m^3 s^{-1}. The mean upwelling velocity and the vertical diffusivity, in the 3000–4500 m depth range, are estimated as 3×10^6 m s^{-1} and 2.5×10^{-4} m^2 s^{-1}, respectively. The results also suggest faster upwelling in the western Indian Ocean.

1. Introduction

The global overturning circulation driven by air-sea exchange of heat and salt, consists of the formation of cold, dense deep and bottom waters at high latitudes in the North Atlantic and the Southern Ocean, their export to low latitudes with a gradual warming and upwelling en-route, and finally a compensating return of waters to the areas of formation at shallower depths. It has been known for some time now that the deep Indian Ocean, as a part of this circulation, essentially transforms cold and dense bottom waters imported from the south into warmer and lighter waters (Reid and Lynn, 1971; Warren, 1981; Stuiver *et al.,* 1983). The magnitude of this circulation, however, has proved difficult to determine. Conventional geostrophic transport calculations suggest a vigorous deep circulation (Warren, 1981; Toole and Warren, 1993). The estimated upwelling rate of 15–25 m yr^{-1} is three to five times the upwelling rate estimated for the Pacific Ocean. With both Pacific and Indian oceans forming the upwelling limb of the global overturning circulation, the results imply an equivalent net upward flux of deep water in the Indian and in the much larger Pacific Ocean. In recent years, special attention has been given to the Indian Ocean in an effort to verify the deep upwelling rate in this ocean (Robbins and Toole, 1997; Lee and Marotzke, 1997; McCarthy *et al.,* 1997; You, 1999). These studies suggest a significantly lower upwelling rate, with estimates ranging from 1 to 10 m yr^{-1}. Thus despite several

1. Rosenstiel School of Marine and Atmospheric Sciences, University of Miami, Miami, Florida, 33149-1098, U.S.A. ***email: asrinivasan@rsmas.miami.edu***

attempts, the upwelling rate in the Indian Ocean is still not well constrained by observations. The purpose of this work is to re-examine the radiocarbon distribution in order to provide an independent estimate of the abyssal upwelling rate in the Indian Ocean.

Stuiver *et al.* (1983) used the GEOSECS radiocarbon data in the context of a global box-model. The results suggested an upwelling rate of 10 m yr^{-1}, two times the upwelling rate for the Pacific Ocean at the 1500 m level. The box-model is simple and easy to implement but does not consider the processes responsible for shaping the radiocarbon distribution explicitly. Box-model estimates can be improved by considering the various processes important for the distribution of radiocarbon explicitly. This is done in the analysis presented here by using an advection-diffusion model.

The deep Indian Ocean is partitioned into a number of smaller basins by a complex topography below roughly 2500 m (Fig. 1, Fisher *et al.,* 1982). In this paper, the upwelling in each of these basins is estimated from the observed radiocarbon distribution. A two-layer model is constructed to examine the implications of the vertical distribution of Dissolved Inorganic Carbon (DIC) and its ^{14}C activity for the upwelling rate in each of these basins. The methodology is based on the formulation of the cross-basin integrated tracer conservation equations in a volumetric coordinate system derived from the basin hypsography and the solution of the radiocarbon and heat budget equations. The fact that ^{14}C and DIC distributions are marginally sensitive to the vertical mixing effects allows one to estimate the upwelling transport from ^{14}C budgets based on advective transports and source distributions alone. This solution is also presented and compared with the solution obtained by solving the radiocarbon and heat budget equations.

2. Data and model

Radiocarbon was measured at 23 stations north of 30S in the Indian Ocean (Fig. 1) during the GEOSECS expedition (Stuiver and Ostlund, 1983). The ^{14}C distributions, shown as meridional sections, are presented in Figure 2. Below 2000 m, two major features stand out: (1) There is a general south to north decrease in radiocarbon content in the deep Indian Ocean. (2) The bottom waters (below approximately 3500 m) have a higher radiocarbon content than deep waters (2000–3500 m) and there is a mid-depth (2000–2500 m) minimum in radiocarbon distribution.

These features result from a combination of abyssal circulation, mixing, radioactive decay and radiocarbon sources in the Indian Ocean. Previous studies in the deep basins of the Indian Ocean have discerned a general meridional circulation pattern (Warren, 1974, 1977, 1982; Johnson *et al.,* 1991a,b; Toole and Warren, 1993; Mantyla and Reid, 1995). The circulation is most simply described by a two-layer system consisting of a bottom and deep layer. Southward flow in the deep layer (approximately 2000–3500 m) is replenished by upwelling from the bottom layer and northward transport (below 3500 m) in the bottom layer. A schematic of this circulation pattern is depicted in Figure 3. With this configuration, and including the effects of mixing, sources and sinks, the radiocarbon data are used

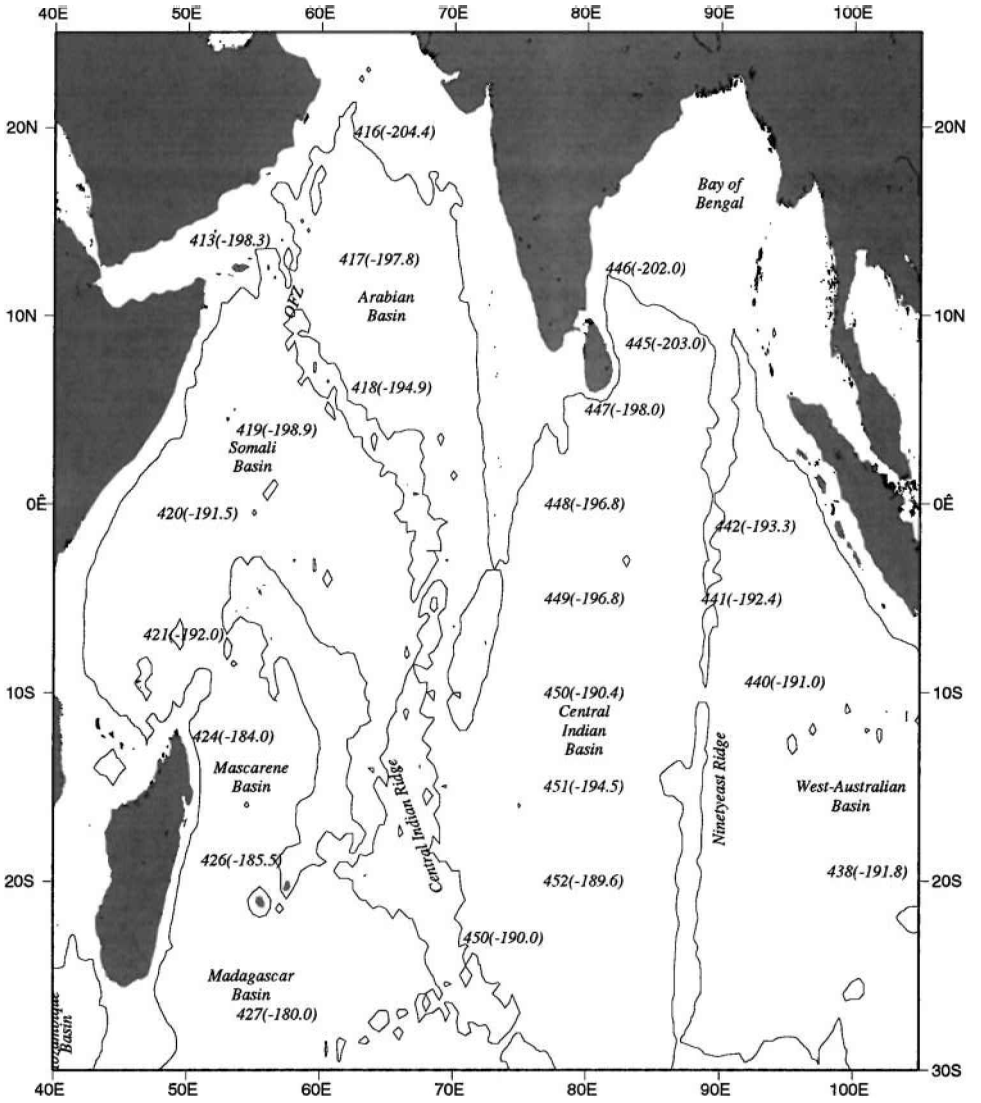

Figure 1. Map of the deep Indian Ocean identifying the important topographic features. Also shown are the GEOSECS stations and the minimum specific radiocarbon activity at each station in per mil. (OFZ: Owens Fracture Zone).

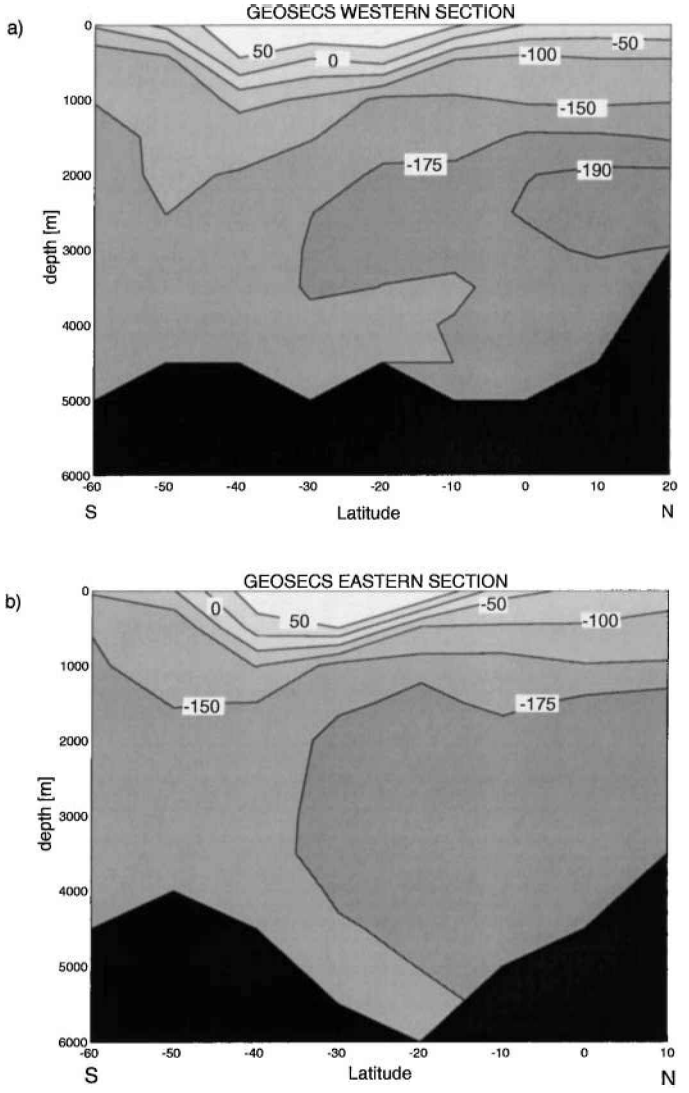

Figure 2. Radiocarbon sections from (a) western and (b) eastern GEOSECS sections. The isolines are in $\Delta^{14}C$ notation. The mid-depth waters have lower values of radiocarbon than the inflowing bottom waters due to decay during the upwelling process.

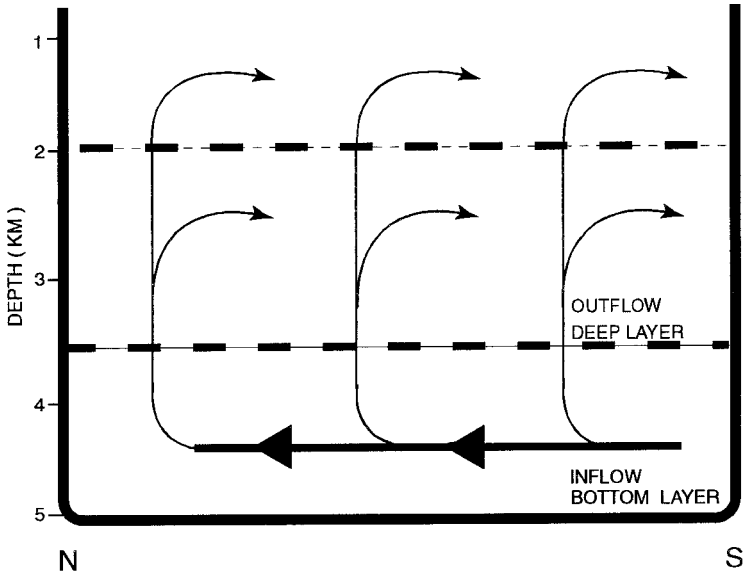

Figure 3. Sketch showing the deep circulation pattern in the Indian Ocean basins. Bottom waters upwell and feed the southward return flow at lesser depths.

to calculate the upwelling transport from the bottom to the deep layer. The above analyses (e.g., Toole and Warren, 1993; Mantyla and Reid, 1995) have also identified the inflow and outflow regions in the deep Indian Ocean. These studies are used here as guidelines to fix layer interfaces for the present analysis. The layers are defined in Table 1. The GEOSECS radiocarbon and carbonate chemistry data from each basin are sorted into bins, corresponding to the two layers, and averaged. The layer averaged alkalinity, DIC and absolute radiocarbon concentration for all the GEOSECS stations and for deep and bottom water layers are listed in Table 1.

3. Characteristics of the binned data

In this section the horizontal and vertical variations in the radiocarbon concentrations are examined. The minimum specific activity at each station, expressed in per mil anomaly on the $\Delta^{14}C$ scale is shown in Figure 1. At a mean activity deficit of $-195‰$, each per mil unit corresponds to 10 years of aging in the system. The regional minimum activity anomaly in each basin deviates from the mean activity anomaly for each basin by no more than 10%. The meridional trends in the vertical gradient of $\Delta^{14}C$ for all the basins are shown in Figure 4. Even with the coarse vertical resolution employed in this study vertical structure dominates over the horizontal variability. In each basin the vertical gradients in $\Delta^{14}C$ are uniform within measurement uncertainty. The mean horizontal variation of $\Delta^{14}C$ within a given layer is less than 30% of the difference between the layers. This distribu-

Table 1 (a). Layer averaged alkalinity, DIC, and absolute radiocarbon for GEOSECS Indian Ocean stations. Neutral density is used to define layer interfaces and was calculated using Jackett and McDougall (1997) routine.

Station	Alkalinity μ eq kg^{-1}	DIC μ mol kg^{-1}	Absolute radiocarbon $\times 10^{-18}$ mol kg^{-1}
	Arabian Basin deep water layer		
	σ_N: 27.95–28.06		
413	2438	2344	1882
417	2425	2339	1886
418	2418	2326	1877
	Somali Basin deep water layer		
	σ_N: 27.95–28.12		
419	2408	2311	1870
420	2415	2316	1878
421	2406	2305	1869
	Madagascar and Mascarene Basins deep water layer		
	σ_N: 27.95–28.13		
424	2398	2297	1884
426	2402	2293	1883
427	2390	2281	1877
	Central Indian Basin deep water layer		
	σ_N: 27.95–28.12		
447	2430	2321	1871
448	2420	2317	1875
444	2423	2302	1861
449	2415	2309	1866
450	2410	2299	1869
451	2405	2291	1856
453	2400	2286	1872
	West Australian Basin deep water layer		
	σ_N: 27.95–28.14		
442	2414	2310	1871
441	2415	2308	1869
440	2403	2308	1867
438	2387	2290	1857
436	2393	2291	1860

Table 1 (b). Layer averaged alkalinity, DIC, and absolute radiocarbon for GEOSECS Indian Ocean stations. Neutral density is used to define layer interfaces and was calculated using Jackett and McDougall (1997) routine.

Station	Alkalinity μ eq kg^{-1}	DIC μ mol kg^{-1}	Absolute radiocarbon $\times 10^{-18}$ mol kg^{-1}
	Arabian Basin bottom water layer		
	σ_N: 28.06–bottom.		
413	—	—	—
417	2437	2337	1901
418	2428	2319	1888
	Somali Basin bottom water layer		
	σ_N: 28.12–bottom.		
419	2403	2294	1884
420	2402	2296	1878
421	2396	2289	1884
	Madagascar and Mascarene Basins bottom water layer		
	σ_N: 28.13–bottom.		
424	2388	2274	1887
426	2398	2283	1897
427	2375	2269	1891
	Central Indian Basin bottom water layer		
	σ_N: 28.12–bottom.		
447	2431	2315	1875
448	2427	2311	1867
444	2418	2307	1866
449	2410	2203	1864
450	2408	2297	1870
451	2417	2293	1850
453	2414	2267	1841
	West Australian Basin bottom water layer		
	σ_N: 28.14–bottom.		
442	2414	2282	1876
441	2415	2284	1875
440	2403	2283	1875
438	2387	2275	1881
436	2387	2278	1891

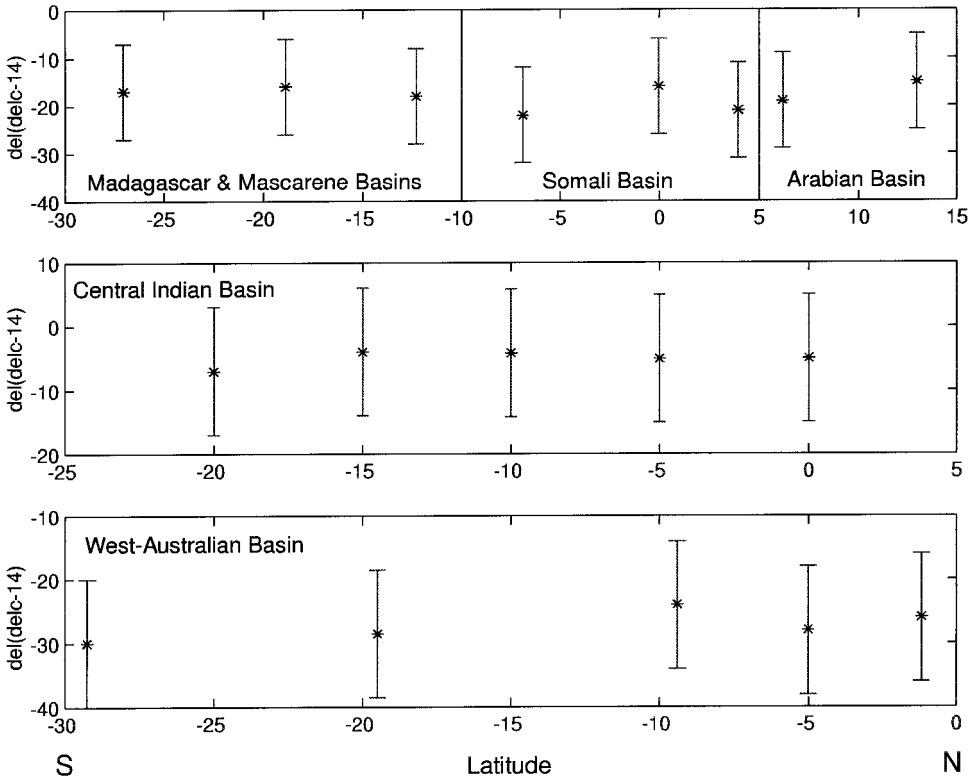

Figure 4. Meridional trends in vertical radiocarbon gradients between the deep and bottom layers in the various basins of the Indian Ocean. The variations are mostly within measurement error. The uniform vertical gradients allow estimation of vertical transfer process using horizontally-averaged radiocarbon concentrations.

tion of radiocarbon in the deep ocean is mainly imposed by its half-life. A scale and order of magnitude analysis can be made to gauge the importance of the various processes acting to distribute radiocarbon in the deep basins. The simplified conservation equation governing the steady-state distribution of radiocarbon for the circulation scheme described above is:

$$vdc/dy + wdc/dz = K_h d^2c/dy^2 + K_z d^2c/dz^2 - \lambda c + J \quad (1)$$

where, v and w are the horizontal and vertical velocities, K_h and K_z are the horizontal and vertical diffusivities, c is the radiocarbon concentration, λ is the radioactive decay constant and J is the particulate source term. The values used below for horizontal and vertical scales are chosen considering the mean individual basin length north of 30S and mean layer thickness, respectively. Canonical values are used for velocities and diffusivities

(e.g., Veronis, 1981; Rhines, 1993) as shown below:

horizontal distance scale:	$y \sim 3000$ km
vertical (depth scale):	$h \sim 1000$ m
horizontal velocity:	$v \sim 1 \times 10^{-3}$ m s^{-1}
vertical velocity:	$w \sim 1 \times 10^{-7}$ m s^{-1}
horizontal diffusivity:	$K_h \sim 1 \times 10^{3}$ m^2 s^{-1}
vertical diffusivity:	$K_v \sim 1 \times 10^{-4}$ m^2 s^{-1}
decay constant:	$\lambda = 5.5 \times 10^{-12}$ s^{-1}

From the above values and observed radiocarbon distribution the order of magnitude of the following quantities for the Indian Ocean, north of 30S, are estimated as:

horizontal advection:	$vdc/dy \sim 2 \times 10^{-26}$ mol kg^{-1} s^{-1}
vertical advection:	$wdc/dz \sim 4 \times 10^{-27}$ mol kg^{-1} s^{-1}
horizontal diffusion:	$K_h d^2c/dy^2 \sim 4 \times 10^{-27}$ mol kg^{-1} s^{-1}
vertical diffusion:	$K_v d^2c/dz^2 \sim 5 \times 10^{-28}$ mol kg^{-1} s^{-1}
radioactive decay:	$\lambda c \sim 1 \times 10^{-26}$ mol kg^{-1} s^{-1}
particulate input:	$J \sim 8 \times 10^{-27}$ mol kg^{-1} s^{-1}.

Evidently, particulate input approximately balances radioactive decay in the deep Indian Ocean. This input can be removed from the background radiocarbon distribution by considering changes in dissolved inorganic carbon. The details of this process are described later in Section 4. The radiocarbon gradients and their derivatives are calculated by removing the particulate input from the observed concentration. In the absence of particulate input, radiocarbon decay is approximately balanced by horizontal advection, while vertical advection is an order of magnitude smaller than decay. Diffusion plays a secondary role in balancing radioactive decay in both horizontal and vertical direction. Therefore, horizontal gradients within a given layer are small and there is clear vertical separation of the bin averages for the two layers. This pattern suggests that basin-wide vertical processes may be reasonably approximated in terms of horizontally averaged properties and fluxes. The regional variability in each basin can then be treated as perturbations on the mean basin-wide vertical processes. Significant errors in such an approach could arise from regional variations in the mixing processes if the latter were correlated with the local deviations of the vertical property gradients from their basin means. The approximate basin scale uniformity of the vertical gradients, however, largely excludes this possibility (Fig. 4).

In the case of the central Indian Basin the deep waters between 2000–3500 m are imported directly from the south, whereas bottom waters (below 3500 m) are derived from the West-Australian Basin through gaps in the Ninetyeast Ridge (Warren, 1982; Toole and Warren, 1993; Talley and Baringer, 1997). Therefore, the deep waters of the central Indian Basin are not significantly older than the bottom waters and both deep and bottom waters

have comparable radiocarbon contents. For this reason a slightly different construction, described later, is used to estimate upwelling in this basin.

4. The diagnostic equations

The upwelling from the bottom into the deep layer is diagnosed based on a radiocarbon budget for the deep layer. The radiocarbon loss (due to radioactive decay) in the deep layer is balanced primarily by upwelling transport of radiocarbon from the bottom layer. Diffusive transports (both horizontal and vertical) of radiocarbon are expected to play only a minor role in balancing the radiocarbon loss in the deep layer. This is verified later by comparing the diffusive transport of radiocarbon and the radiocarbon deficiency for the deep layer. In view of the approximate horizontal uniformity in the radiocarbon concentrations within layers (Fig. 4), horizontally averaged radiocarbon concentrations are used to calculate transports. In this section, the approximations made by treating the problem as one of horizontally averaged properties and fluxes are considered, and the specific transport equations used in the diagnostic analysis are set up.

Let any conservative tracer concentration C, on a horizontal surface spanning a basin be $C = \{C\} + C'(x, y) + C''(x, y, t)$, where the spatial mean of C' (the regional deviations from the mean concentration on the horizontal surface) and the temporal mean of C'' (the temporal deviations from the mean concentration on the horizontal surface) are identically zero and curly brackets denote the mean tracer concentration. A vertical eddy diffusivity $K = \{K\} + K'$ is defined by the diagnostic equation

$$-\{W''C''\} = \{K\}\{C_Z\} + \{K'C'_Z\}. \tag{2}$$

Here W is the vertical velocity defined as positive upward. $\{W''C''\}$ is thus, the turbulent vertical tracer transport parameterized in terms of a spatially constant $\{K\}$ and a spatially variable K'. The total vertical transport of C, area normalized and neglecting molecular diffusion across this surface, is given by:

$$\{WC\} = \{W\}\{C\} - \{K\}\{C_Z\} - [\{W'C'\} + \{K'C'_Z\}]. \tag{3}$$

The square-bracketed terms on the right-hand side of Eq. 3 represent macro-scale correlation, which cannot be neglected *a priori*. However, they are only of secondary concern in the present case due to substantial uniformity in the vertical gradients of the ^{14}C field (Fig. 1; Fig. 4). Denoting the basin area by $S(Z)$ and focusing on the basin-wide water transport, the total upwelling transport is given by $S(Z) \times \{W\} = T$. The total flux F_C, of any tracer measured by C across any horizontal level is then:

$$F_C = T\{C\} - S\{K\}\{C_Z\}. \tag{4}$$

This equation is applied to the interface separating the two layers to calculate upwelling from the bottom layer to the deep layer.

In order to treat nonconservative tracers like radiocarbon, sources and sinks must be considered. The budget equation involves first of all a decay term for radiocarbon. In

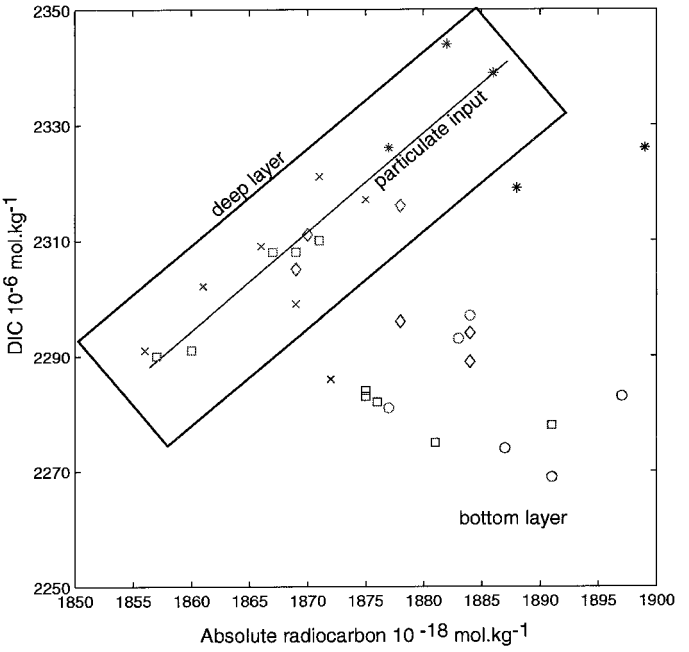

Figure 5. Plot of absolute radiocarbon and DIC for all basins. Data were binned into deep and bottom layers. Particulate origin radiocarbon is mainly added to the deep layer (delineated by the rectangle in the figure). This is also evident from the approximately linear relationship between deep layer radiocarbon and DIC. (Asterisks—Arabian Basin, Diamond—Somali Basin, Circle—Madagascar and Mascarene Basins, cross—Central Indian Basin, square—West-Australian Basin)

addition, biogenic carbon sedimentation and dissolution must be considered (Craig, 1969). The latter may occur either during the settling process or at the bottom sediment interface. The biogenic carbon source will also appear as a source term for radiocarbon since surface biota grow in an environment of ^{14}C activity different from the abyssal water values. A plot of absolute radiocarbon versus DIC for both layers is shown in Figure 5; it reveals the effects of biogenic sedimentation and dissolution in the two-layer model of the deep Indian Ocean. Here, absolute radiocarbon is defined as $R \times DIC$ where $R = 1 + 10^{-3} \times \Delta^{14}C$ is a measure of specific ^{14}C activity (Broecker and Peng, 1982). The mole fraction of ^{14}C in the oceanic carbon reservoir is close to 10^{-12} and DIC units are 10^{-6} mol kg^{-1}. Therefore, absolute radiocarbon values are reported as multiples of 10^{-18} mol kg^{-1}.

The balance between upwelling from the bottom layer and oxidation and dissolution of sinking particles increases the DIC content of the deep layer. For the deep layer, radiocarbon concentration increases approximately linearly with increase in DIC, reflecting its particulate origin (Fig. 5). Furthermore, the difference between absolute radiocarbon concentrations for the deep and bottom layer suggests that particulate input approximately balances the loss of radiocarbon during upwelling due to radioactive decay. Another important point to note in Figure 5 is the fact that particulate transport to the bottom layer is

significant only in the Arabian Basin. This is due to the high productivity of the Arabian Basin surface waters (e.g., Koblentz-Mishke, 1970). The increased transport of particulate matter to the deep Arabian Basin leads to a higher DIC content in the bottom waters of the Arabian Basin (e.g., Broecker *et al.,* 1980).

The effects of biogenic radiocarbon input can be removed by considering changes in alkalinity and DIC. Let the biogenic carbon sedimentation rate across any level Z be G. The specific activity of biogenic source is possibly depth dependent. The primary reason why it may vary with depth has to do with the relative significance of *in situ* oxidation or dissolution of settling particles and of processes at the sediment-water interface. While the former processes may be expected to render DIC with the same activity as the surface waters, the latter process may suffer from the influence of a much delayed dissolution of carbonates. To deal with this difference, the biogenic carbon sedimentation rate is considered to consist of three components, namely, an organic carbon flux G_o and two carbonate sources G_a and G_{ab}. The latter two are assumed to reach the bottom, where G_a undergoes dissolution while G_{ab} represents the rate of sediment accumulation. G_{ab} is not accessible to water column diagnostics but G_a may be inferred from its effect on alkalinity. The organic matter oxidation is assumed effectively instantaneous (Broecker and Peng, 1982). Accordingly, G_o is assigned an activity level R_o assumed to be effectively the same as the surface mixed layer. The carbonate dissolution flux is assigned a value $R_a < R_o$, thus allowing for aging of this source during dissolution at the top surface of the sediment layers. For the purpose of integral budgets it is clear that of the total biogenic carbon flux R_oG, the fraction that contributes to water column balance is equal to $R_oG_o + R_aG_a$. The bracket notation is discarded below where analyses are done using layer averaged variables and the total fluxes are calculated for the entire basin.

The layer averaged alkalinity is denoted by A, DIC by B, and the effective radiocarbon concentration R $\times$ DIC by C. With the above notations the total balance equations for the deep layer are:

$$T(A - A_b) = SKA_Z + 2G_a \tag{5}$$

$$T(B - B_b) = SKB_Z + G_o + G_a \tag{6}$$

$$T(C - C_b) = SKC_Z + R_oG_o + R_aG_a - \lambda \int CSdz \tag{7}$$

where A_b, B_b, and C_b are the bottom layer concentrations, T is the net upwelling transport, S is the area of the interface between the deep and bottom layers and λ is the radioactive decay constant for radiocarbon. The factor 2 in the alkalinity equation (5) arises due to charge balance considerations. This system of equations can be simplified for diagnostic purposes by defining an adjusted radiocarbon concentration $C^* = C - R_oB + 0.5(R_o - R_a)A$. Substitution in (7) yields:

$$T(C^* - C_b^*) - SKC_Z^* = -\lambda \int C^*SdZ. \tag{8}$$

Eq. 8 is the basis of the following diagnostics. It is applied to a control volume that has the mid-point of the bottom layer as the lower boundary and the mid-point of the deep layer as

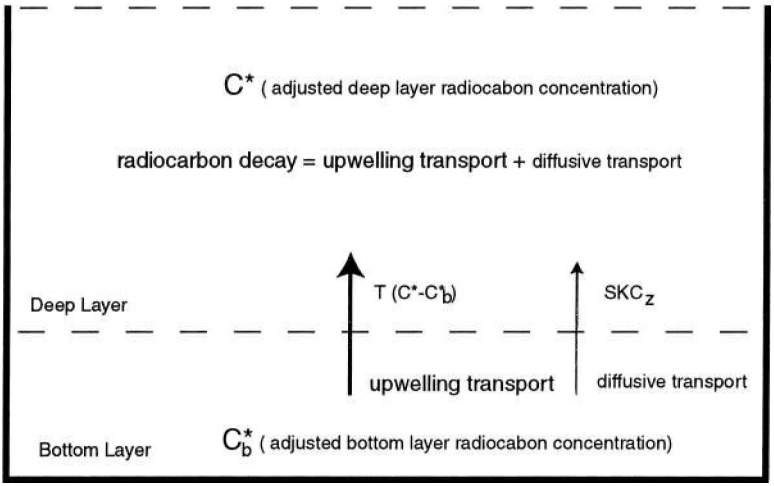

Figure 6. Diagram showing the important processes which influences the radiocarbon budget in the deep layer. In the absence of particulate input, the radiocarbon decay in the deep layer is mainly balanced by upwelling transport of radiocarbon from the bottom layer.

the upper boundary. Considering that the value of C^* anywhere in the world ocean deviates from its mean by no more than 20%, the right-hand side of Eq. 8 can be thought of approximately as a basin geometry-dependent forcing term for the distribution of C^*. The various terms involved in the radiocarbon budget for the deep layer are shown in Figure 6. The adjusted radiocarbon concentration defined here is the background radiocarbon obtained by removing biogenic radiocarbon input. Values for C and C^* are shown in Table 2, estimated as layer means for the data in Table 1. The meridional trend in C^* for both layers is displayed in Figure 7.

In the case of central Indian Basin, at station 453 there is significantly higher radiocarbon than in the interior. This station is located on the southwestern boundary of the

Table 2. Mean deep and bottom water layer alkalinity, DIC, absolute radiocarbon and adjusted absolute radiocarbon for all the basins. Deep layer values are listed above the bottom layer values.

Basin	A μ eq kg^{-1}	B μ mol kg^{-1}	C $\times 10^{-18}$ mol kg^{-1}	C* $\times 10^{-18}$ mol kg^{-1}
Arabia Basin	2427	2336	1882	1803
	2433	2328	1895	1829
Somali Basin	2410	2311	1872	1818
	2400	2293	1882	1850
Madagascar & Mascarene	2397	2290	1881	1846
Basins	2387	2275	1892	1876
Central Indian Basin	2417	2307	1866	1832
	2414	2304	1865	1844
West-Australian Basin	2402	2301	1865	1816
	2401	2280	1880	1860

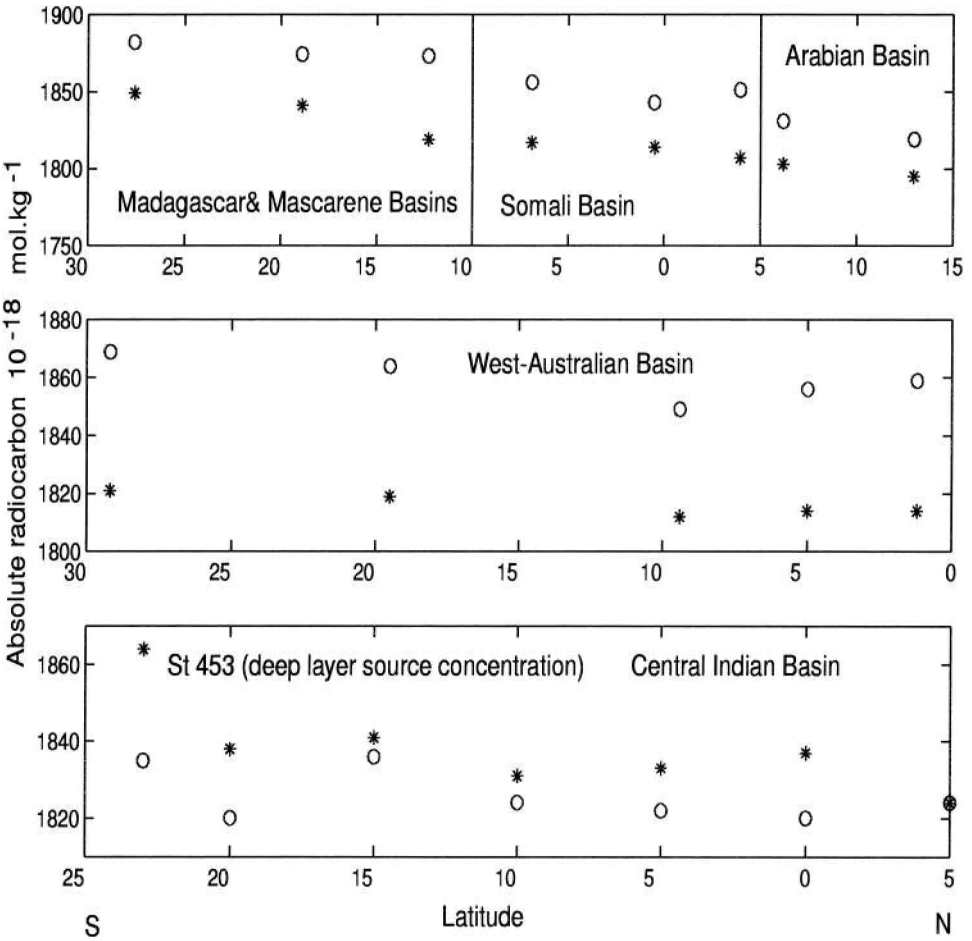

Figure 7. Meridional trend in adjusted radiocarbon in the deep Indian Ocean. The circles and the asterisks represent the bottom and deep layers, respectively. The clear vertical separation and small variations within layers allows quantification of vertical transfer process using layer-averaged concentrations. In the case of the central Indian Basin the deep layer has a higher radiocarbon concentration. This is due to the source (see text) located in the southwest corner and within the deep layer.

basin, and within the core of the boundary current supplying water to this basin. The radiocarbon content at this station is chosen as representative of source waters, that is C_b^*, for the central Indian Basin. However, the bottom layer radiocarbon concentrations are used to correct for the diffusive transport of radiocarbon.

In the following diagnostics a value of 0.95 for R_o as well as for R_a is used. Results for $R_a = 0.3$ are also presented to indicate the sensitivity of the model to carbonate dissolution. The assignment of an appropriate value for the biogenic radiocarbon activity is complicated by anthropogenic ^{14}C. Due to the brevity of the anthropogenic influence epoch

compared with the abyssal circulation and ventilation time scales, one might assume that its effect on the abyssal radiocarbon budgets is small. The value of 0.95 corresponds to estimates of surface equilibration of ^{14}C before the nuclear era (Broecker and Peng, 1982). It is chosen in view of the long averaging time scale involved in the abyssal transport processes. Choosing a value of $R = 1.1$ for a period of 20 years, and 0.95 for 400 years yields a gross average of 0.96. Compared to interior values of R of $O(0.8)$, this implies a 6% adjustment in $(C^* - C_b^*)$ which is not significant in view of the overall precision in C estimates. The observed range of R values in the layer bins for each basin is around 2–3 times the counting precision of 3–4‰, and sample numbers range from 4 to 10. Since biogenic input is only 1% of the background DIC, a 10% uncertainty in its source activity is effectively masked by the combination of natural variability and counting limitations.

5. Transport and diffusivity diagnostics

a. Significance of the diffusion term and upwelling in the advective approximation

Eq. 8 states that at steady state the radiocarbon lost due to decay in the deep layer is balanced by upwelling and diffusive transport of radiocarbon. Since C^* has a minimum at the top of the deep layer around 2000 m (Fig. 2; Fig. 8), diffusion across the top of the upper layer can be neglected. Therefore, radioactive decay in the deep layer is balanced by upwelling and diffusion from the bottom layer. The significance of the diffusion in this process can be gauged by comparing the decay integral on the right-hand side of Eq. 8 to the diffusive transport under a reasonable approximation of the layer-averaged vertical diffusivity. The decay integral in Eq. 8 is calculated using the estimates for volume of the deep layer and area of the interface between the layers given in Table 3. These estimates are derived from values tabulated by Levitus (1994). The decay integral and diffusive transport for each basin calculated choosing a value of 10^{-4} m^2 s^{-1} for diffusivity are listed in Table 4. The diffusion of tracer from bottom to deep layer is less than 15% of the decay integral for the deep layer, except for the West-Australian Basin where it is 18.5%. Therefore, diffusion plays a secondary role in balancing the tracer budget. A rough, advective estimate for upwelling can be derived by neglecting diffusion from the bottom layer to the deep layer. The upwelling transport for each basin in the advective approximation and the mean upwelling velocity are listed in Table 4. The net upwelling transport including all the basins is 9.9×10^6 m^3 s^{-1}. In the next section a better estimate is obtained and compared with the rough estimate obtained in this section.

b. Transport and diffusivity estimates

The radiocarbon balance equation (Eq. 8) has two unknown quantities: upwelling transport and diffusivity. Heat budget considerations give a similar equation with these unknowns. The integral heat balance below the upper layer is given by:

$$T(q_p - q_s) = S(Kq_{P,Z} + Q) \tag{9}$$

where q_p is the potential temperature, q_s, the potential temperature of the source, and Q is

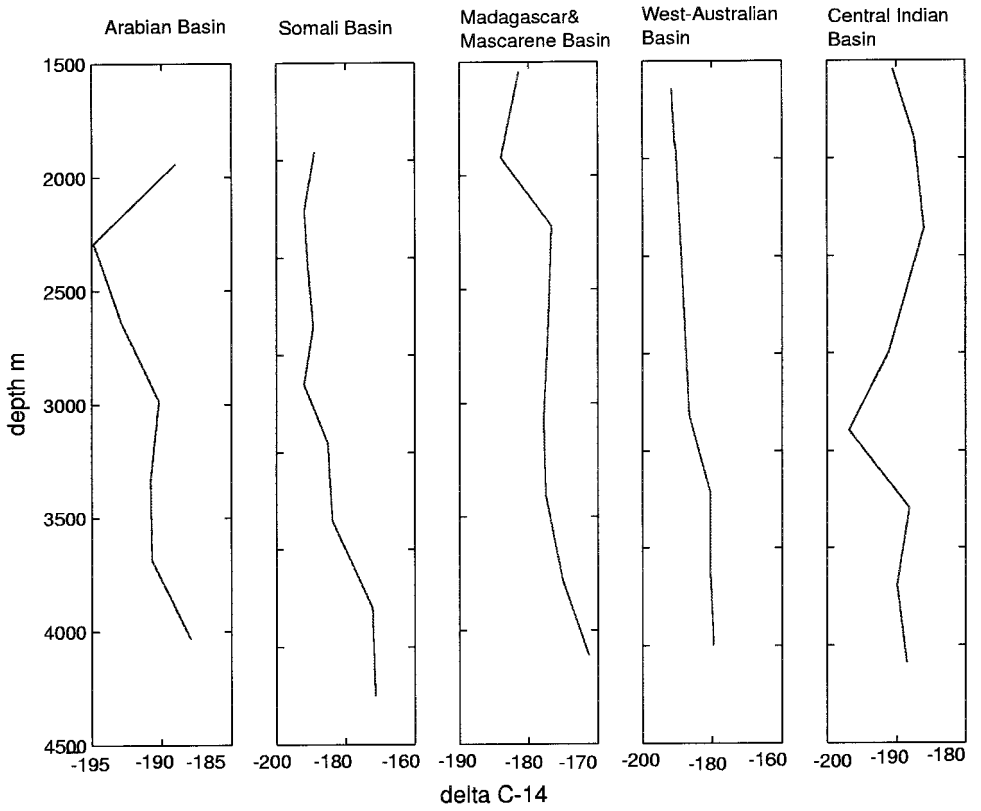

Figure 8. Mean vertical radiocarbon profiles in each deep basin. There is a minimum around 2000 m in each basin. Again, in the central Indian Basin the deep layer has a higher radiocarbon concentration due to the source located on the southwest corner in the deep layer.

the geothermal heat flux per unit bottom area projected onto a level surface. Eqs. 8 and 9 can be solved to obtain the transport and diffusivity estimates.

Table 5 lists the quantities used for the heat budget equation. Historical data from Mantyla and Reid and the recent WOCE data are used for the basin-averaged potential

Table 3. Basin hypsography and the deep water layer volume for the Indian Ocean basins considered in this analysis derived from Levitus atlas (1994).

Basin	Area 10^{12} m^2 2000 m	3000 m	4000 m	Volume 10^{15} m^3
Arabian Basin	3.8	3.2	1.0	2.8
Somali Basin	5.7	5.1	2.7	9.7
Madagascar & Mascarene Basins	4.7	4.2	2.7	8.1
Central Indian Basin	8.3	7.2	5.3	15.0
West-Australian Basin	9.7	8.4	7.4	18.0

Table 4. Decay integral and transport diagnostics in the advective approximation. Diffusive transport is calculated choosing a diffusivity of 1×10^{-4} m^2 s^{-1}.

Basin	Decay integral $\times 10^{-12}$ mol kg^{-1}	Diffusive transport $\times 10^{-12}$ mol kg^{-1}	Upwelling flux $\times 10^{6}$ m^3 s^{-1}	Mean W $\times 10^{-7}$ m s^{-1}
Arabian Basin	19.3	3.9	0.7	2.5
Somali Basin	62.5	4.5	1.9	4.2
Madagascar & Mascarene Basins	60.4	3.7	2.0	5.0
Central Indian Basin	97.8	13.5	3.0	4.4
West-Australian Basin	100.6	18.5	2.3	2.8

temperature and source potential temperatures. A canonical value of 50 mW m^{-2} (Anderson *et al.,* 1977) is used for the geothermal heat flux. Vertical profiles of temperature for each basin are shown in Figure 9. The estimated upwelling transport and the diffusivity and the mean upwelling velocity for each basin are listed in Table 6. From Table 6 the net upwelling transport is 8.5×10^6 m^3 s^{-1}. This represents an ~15% decrease compared with the upwelling estimate in the advective approximation. This reduction is due to the contribution of the diffusive transport of radiocarbon from the bottom layer to the deep layer. In the next section, the model sensitivity to delayed dissolution of carbonate is tested.

c. Model sensitivity to carbonate dissolution

In the analysis presented above the organic and inorganic DIC sources were not separated. A value of 0.95 for the specific activity of the radiocarbon source due to particulate input was assumed. To study the effects of delayed dissolution of carbonate and consequently lower specific activity of the inorganic radiocarbon source on the transport estimates, a value of 0.3 is chosen for R_a. The results are shown in Table 7. Upwelling estimates in individual basins are increased by less than 30% and for the entire Indian Ocean by approximately 10%. In general, the inorganic contribution to DIC reduces the radiocarbon gradients between the deep and bottom layers, which leads to an increase in the calculated upwelling transport. The central Indian Basin shows a small decrease in

Table 5. Various quantities used for the heat budget equation. Historical data and the WOCE data were used to estimate these quantities.

Basin	Mean q °C	Source °C	dq/dz °C m^{-1}
Arabian Basin	1.47	1.30	6×10^{-4}
Somali Basin	1.12	0.85	4×10^{-4}
Madagascar & Mascarene Basins	0.98	0.65	5×10^{-4}
Central Indian Basin	1.54	1.12	6×10^{-4}
West-Australian Basin	0.84	0.60	4×10^{-4}

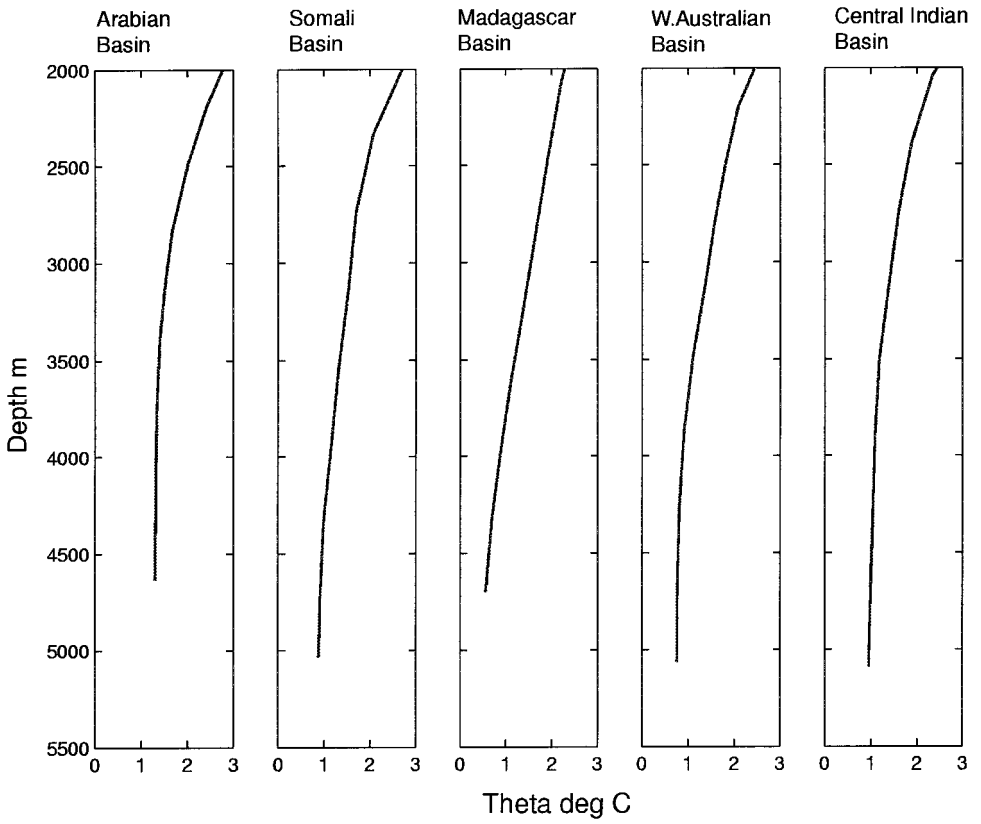

Figure 9. Mean vertical temperature profiles in the deep basins. These profiles were used to correct for the effects of mixing on the upwelling transports diagnosed from radiocarbon data. Historical data from Mantyla and Reid and the WOCE data were used for generating these profiles.

upwelling compared to the other basins since only the deep water concentrations are used in the diagnostics.

6. Limitations of the analysis

Three distinct points are addressed in this section, namely, the assumption of process steadiness, the question of errors arising from the neglect of correlation terms like $\{K'C'_Z\}$, and mixing between deep waters of the various deep basins.

The diagnostics presented here are based on the observed gradients in the radiocarbon concentration between the bottom and deep layers. The impact of variations in the circulation on the diagnostic estimates is best addressed by considering the changes in gradients that would result from variability in the circulation. For example, if the circulation were accelerated, the gradients between the layers would be reduced. On the other hand, if the circulation is decelerated, then the gradients would be increased given the

Table 6. Upwelling and diffusive transport estimates. Diffusive transport is calculated using the estimated diffusivity.

Basin	Decay integral $\times 10^{-12}$ mol kg^{-1}	Diffusivity $\times 10^{-4}$ m^2 s^{-1}	Diffusive transport $\times 10^{-12}$ mol kg^{-1}	Upwelling flux $\times 10^6$ m^3 s^{-1}	Mean W $\times 10^{-7}$ m s^{-1}
Arabian Basin	19.3	1.7	3.9	0.6	2.0
Somali Basin	62.5	3.5	4.5	1.5	3.2
Madagascar & Mascarene Basins	60.4	3.5	3.7	1.6	4.0
Central Indian Basin	97.8	2.5	13.5	2.7	3.9
West-Australian Basin	100.6	0.9	18.5	1.8	2.2

long half-life of radiocarbon. The approximate adjustment time scale should be the advection or equivalently the ventilation time. From the data in hand, the ventilation time for the Indian Ocean is roughly 300 years (e.g., Stuiver *et al.,* 1983). Significant variability on this mean time scale would be expected to introduce detectable deviations (greater than the measurement precision of 3.5‰) from the simple vertical structure on the 2000 m scale of the primary model domain (Fig. 8). The absence of such deviations and the good fit obtained for the diagnostic computations suggest that the circulation has been steady for the last 300 years. The resolution used in binning the data is roughly consistent with the fact that the diffusive scale length, $H = \{K\}/\{W\}$, deduced from the estimated transport parameters ranges from 500 to 1000 m. Thus, gradient aliasing of the vertical fine structure should not be a problem in this argument. Therefore, the current estimate can be taken to be averaged over the last 300 years. Further analysis of this problem will be possible when the WOCE radiocarbon results become available.

Error sources related to the horizontal variations in property gradients (that is, due to neglect of square-bracketed terms in Eq. 3) are likely to be significant in the central Indian Basin. The central Indian Basin has a direct source of upper deep water, through a boundary current along the central Indian Ridge, and an indirect source for the bottom water from the West-Australian Basin through gaps in the Ninetyeast Ridge (Warren,

Table 7. Model sensitivity analysis with $R_a = 0.30$.

Basin	Upwelling transport $R_a = 0.95$	Upwelling transport $R_a = 0.30$
Arabian Basin	0.6	0.7
Somali Basin	1.5	1.9
Madagascar & Mascarene Basins	1.6	2.1
Central Indian Basin	2.7	2.6
West-Australian Basin	1.8	2.0

1981). The transport into the Central Indian Basin for the upper deep water layer is estimated using the concentration gradient between the source waters located on the southwestern boundary and the interior. In this case the source is located in the deep water layer and its input along the meridional span of the basin can lead to horizontal variations in C^* concentration and gradients. However, the near constancy of the interior "adjusted radiocarbon" concentrations suggests that horizontal gradients may be limited to a small area of the basin close to the southern boundary of the basin.

In calculating the radiocarbon budget for the deep layer, horizontal inter-basin tracer transport is not considered. The deep basins are fairly well isolated by the bounding ridges which rise up to approximately 2500 m. Horizontal transport of radiocarbon between basins in the upper 500 m of the diagnostic domain is not likely to affect the radiocarbon budget significantly. For example, the Carlsberg Ridge separating the Arabian and Somali basins offers a porous boundary above ~3000 m. The effect of horizontal transport from the Arabian to the Somali Basin can be calculated from the observed radiocarbon gradients and using 1×10^{-3} m s^{-1} as a scale for the horizontal velocity. The rate of horizontal input into the Somali Basin deep layer across a surface with area equal to the mean width of the Arabian Basin multiplied by the 1000 m is 7.2×10^{-18} mol kg^{-1} s^{-1}. This is insignificant compared to 6.0×10^{-15} mol kg^{-1} s^{-1}, the vertical flux of radiocarbon due to upwelling.

Finally, one might wonder if this analysis would not be better accomplished using the new WOCE radiocarbon data. The GEOSECS radiocarbon data are suited for this analysis by virtue of the sampling period between 1977–1978. Anthropogenic radiocarbon complicates the distribution of radiocarbon in the deep ocean. The effects of bomb radiocarbon in deep waters, added by the fallout to the surface waters, which sink during bottom water formation, can be inferred from the presence or absence of a corresponding tritium signal. However, the effect of bomb radiocarbon component added due to particulate input cannot be easily assessed. Indeed, INDIGO data (Ostlund and Grall, 1988), obtained a decade after GEOSECS, show penetration of the bomb signal deeper into the southwest Indian Ocean. This is probably due to particulate input. The effects of bomb particulate input are likely to be minimal on the GEOSECS data compared to data obtained later. However, the WOCE carbonate chemistry data were used to correct the GEOSECS data. The DIC data from GEOSECS (Weiss *et al.,* 1983) are systematically higher by 21.3 μmol kg^{-1} compared with the latest data (Peng *et al.,* 1998). This systematic offset was subtracted to bring the GEOSECS carbonate chemistry data in line with the recent WOCE data.

7. Implications for the meridional overturning circulation

The immediate significance of the estimate of the net upwelling transport of bottom waters presented here lies in its robust nature; it is independent of assumptions about mixing mechanics and arguably representative of conditions averaged over several centuries. The results therefore complement estimates derived from other methods, namely, geostrophic transport calculations, linear inversion techniques, and Ocean General Circulation Model based estimates. The sum of the bottom upwelling in all the basins is

$8.2 \pm 1.5 \times 10^6$ m^3 s^{-1}. The quoted uncertainty is based on uncertainties in radiocarbon and DIC measurements, which are 3.5‰, and 4 μmol kg^{-1}, respectively. As seen previously, diffusion is only of secondary importance in balancing the radiocarbon budget. It carries a maximum of 25% of the radiocarbon from the bottom layer to the deep layer. Under these conditions the errors in temperature measurements and choice of source and mean temperatures for the layers do not contribute significantly to the errors in the overall transport estimates. On the whole, considering the limitations mentioned above, the error band for the upwelling is probably around 25%.

The present estimate is somewhat smaller than the Robbins and Toole (1997) estimate of $11.9 \pm 2.7 \times 10^6$ m^3 s^{-1}, but compares favorably considering that it does not include the Mozambique Basin, the north Crozet Basin, and the bottom water transport from the West-Australian Basin to the central Indian Basin. You (1999) analyzed the dianeutral transport across four neutral surfaces, and the results show a very weak deep upwelling of 0.2×10^6 m^3 s^{-1} across the deepest neutral surface. You's results show significant upwelling, of 4.6×10^6 m^3 s^{-1}, only in the upper 150 m. On the individual basin scale there are many transport estimates which can be compared with the present estimate. In a recent study, Johnson *et al.* (1999) obtain a value of 2.5 to 3.8×10^6 m^3 s^{-1} for northward transport in the Mascarene Basin. This figure compares well with total vertical flux of 3.7×10^6 m^3 s^{-1} in the three western basins diagnosed in this study. The estimated diffusivity and the vertical velocity are also similar. Johnson *et al.* (1999) estimate a flux of 1 to 1.7×10^6 m^3 s^{-1} through the Amirante Passage into the Somali Basin. Bottom water transport estimate in the Arabian Basin with the WOCE 17N data, and using 1.7°C isotherm as the zero velocity surface, is about 1×10^6 m^3 s^{-1}. These results are similar to values obtained in this study. For the central Indian Basin the estimate of 2.7×10^6 m^3 s^{-1} can be compared with 3×10^6 m^3 s^{-1} calculated by Toole and Warren (1993) for the boundary current transport, but is significantly smaller than 8×10^6 m^3 s^{-1} estimated at 12S in the central Indian Basin by Warren (1981). The estimate of 1.8×10^6 m^3 s^{-1} for the West-Australian Basin is lower than a previous estimate of 6×10^6 m^3 s^{-1} by Toole and Warren (1993). In fact, the large inflow obtained by Toole and Warren (1993) is most probably due to an overestimate of the inflow into the Perth Basin and the West-Australian Basin.

A remarkable aspect of the present estimate is the relatively fast turnover rate for the western Indian Ocean and the associated vertical diffusivity. McCarthy and Talley (1999) come to the same conclusion based on distribution of potential vorticity on neutral surfaces, which reveals a stronger tilt of the potential vorticity isopleths in the western basins, implying stronger circulation in these basins. Studies in the Brazil Basin (Polzin *et al.,* 1997) have indicated many orders of magnitude increase in the diffusivity over rough topography. The smaller basins of the western Indian Ocean have a greater volume fraction exposed to rough topography. The resulting basin-averaged vertical diffusivity is higher than the rest of the Indian Ocean. This enhanced mean vertical diffusivity would then

require a greater upwelling to balance the downward diffusion of heat to maintain the steady state temperature field (Munk, 1966).

A rough idea about the magnitude of the upwelling in the Indian Ocean can be obtained by considering the global upwelling and downwelling fluxes. Whitworth *et al.* (1999) report results from the direct measurements of the deep western boundary current in the Southwest Pacific and use the results to summarize the global downward and upward fluxes of deep waters. Their results and discussions are used here to gauge the magnitude of inflow into the Indian Ocean. The global downwelling fluxes suggest a maximum bottom and deep water production of 28×10^6 m^3 s^{-1}. The recent direct measurements in the Pacific reported by Whitworth *et al.* (1999) give an upwelling flux of 13×10^6 m^3 s^{-1} north of 30S. This figure, when added to 1×10^6 m^3 s^{-1} estimated to upwell in the Atlantic, gives the upper bound for the upwelling flux in the Indian Ocean as 14×10^6 m^3 s^{-1}. The actual inflow is likely to be substantially less than this value due to overestimation of the downwelling flux (see Whitworth *et al.,* 1999 and Broecker *et al.,* 1999). Furthermore, the upwelling north of 30S will be less than 14×10^6 m^3 s^{-1} by an amount that upwells between 30S and the Antarctic Circumpolar Current region. Therefore, most available upwelling estimates seem to be on the higher side.

The present analysis extends the previous box-model radiocarbon estimate in two ways: (1) the use of absolute radiocarbon minimizes the complications due to particulate input, and (2) both advective and diffusive processes are considered in this calculation. These modifications result in a reduction in the upwelling estimates. While the reduced estimate appears to be a step in the right direction, it is not entirely consistent with direct measurements. As a part of the WOCE, current meters were moored across the three main DWBC systems in the Madagascar, Central and West-Australian basins. Preliminary results from the mooring in the Madagascar Basin suggest very little northward transport, while the moorings from the other two basins were not recovered (Warren, personal communication). The northward flow in the Madagascar Basin was found at a much greater depth than previously conjectured from water property distributions. Further analysis of this inconsistency will be possible when the final results from the recovered moorings are available. It is also possible that there was considerable flow in the Central and West-Australian basins, but this cannot be confirmed since the moorings at these sites were lost. Nevertheless, it is important to note that the radiocarbon estimate is averaged over a longer period of time (~300 years) compared with the two-year record of direct measurements.

Recently, Broecker *et al.* (1999) suggest a slowdown of Southern Ocean deep water formation. Broecker *et al.* (1999) using chloroflurocarbon-11 inventories estimate 5×10^6 m^3 s^{-1} deep water production rate in the Southern Ocean. These results conflict with the estimates obtained based on global distributions of radiocarbon and PO_4^* (a conservative tracer defined as $PO_4^* = PO_4 + O_2/175 - 1.95$ μmol kg^{-1}). Broecker *et al.* (1999) argue that this mismatch between short-term (chloroflurocarbon-11) and long-term (radiocarbon and PO_4^*) estimates is due to a slowdown of the deep water production rate in the 20th century. If this were true then it would help reconcile the apparent inconsistency

between the long-term estimate presented here and the results from direct measurements. In such a scenario, the difference in upwelling obtained by the two estimates may simply reflect the temporal variability of the deep water formation in the Southern Ocean. In any case, the present analysis suggests an O (10×10^6 m^3 s^{-1}) inflow of bottom waters across 30S into the Indian Ocean averaged over approximately the last 300 years. The corresponding area-averaged upwelling rate is about 10 m yr^{-1}.

Acknowledgments. Support for this work was provided by NSF grant OCE-9413158. We thank Drs. Rana Fine, William Johns and two anonymous reviewers for comments and suggestions that helped improve the manuscript.

REFERENCES

Anderson, R. N., M. G. Langseth and J. G. Schilater. 1977. The mechanics of heat transfer through the floor of the Indian Ocean. J. Geophys. Res., *82,* 3391–3409.

Broecker, W. S. 1981. Geochemical tracers and ocean circulation, *in* Evolution of Physical Oceanography, B. A. Warren and C. Wunch, eds., MIT Press, Cambridge, 434–460.

Broecker, W. S. and T.-H. Peng. 1982. Tracers in the Sea, Lamont-Doherty Geological Observatory, Palisades, NY, 690 pp.

Broecker, W. S., S. Sutherland and T.-H. Peng. 1999. A possible 20th-century slowdown of Southern Ocean Deep Water Formation. Science, *286,* 1132–1135.

Broecker, W. S., J. R. Toggweiler and T. Takahashi. 1980. A major nutrient source for the deep Indian Ocean. Earth Planet. Sci. Lett., *49,* 506–512.

Craig, H. 1969. Abyssal carbon and radiocarbon in the Pacific. J. Geophys. Res., *74,* 5491–5506.

Fisher, R. L., M. Z. Janstch and R. L. Comer. 1982. Scientific coordinators, General Bathymetric Chart Of The Oceans (GEBCO), Sheet 5.05, Canadian Hydrographic Service, Ottawa.

Jackett, D. R. and T. J. McDougall. 1997. A neutral density variable for the world's oceans. J. Phys. Oceanogr., *27,* 237–263.

Johnson, G. C., B. A. Warren and D. B. Olson. 1991a. Flow of bottom water in the Somali Basin. Deep Sea Res., *38,* 637–652.

—— 1991b. A deep boundary current in the Arabian Basin. Deep Sea Res., *38,* 653–661.

Johnson, G. C., D. L. Musgrave, B. A. Warren, A. Ffield and D. B. Olson. 1999. Flow of bottom and deep water in the Amirante Passage and Mascarene Basin. J. Geophys. Res., *103,* 30973–30985.

Koblentz-Mishke, O. J., V. V. Volkovinsky and J. G. Kabonova. 1970. Plankton primary production of the world ocean, *in* Scientific Exploration of the South Pacific, W. S. Wooster, ed., National Academy of Sciences, Washington, DC, 183–193.

Lee, T. and J. Marotzke. 1997. Inferring meridional mass and heat transports of the Indian Ocean by fitting a general circulation model to climatological data. J. Geophys. Res., *102,* 10585–10602.

Levitus, S. 1994. World Ocean Atlas. CD-ROM data set documentation, NODC Ocean Climate Laboratory, Washington, D.C., Informal report No 13.

Mantyla, A. W. and J. L. Reid. 1995. On the origins of deep and bottom waters in the Indian Ocean. J. Geophys. Res., *100,* 2417–2439.

McCarthy, M. C., L. D. Talley and M. O. Baringer. 1997. Deep upwelling and diffusivity in the southern Central Indian Basin. Geophys. Res. Lett., *24,* 2801–2804.

McCarthy, M. C. and L. D. Talley. 1999. Three-dimensional isoneutral potential vorticity structure in the Indian Ocean. J. Geophys. Res., *104,* 13251–13267.

Munk, W. 1966. Abyssal recipes. Deep Sea Res., *13,* 707–730.

Ostlund, G. H., W. S. Broecker, H. Craig and D. Spencer. 1987. GEOSECS Atlantic, Pacific and Indian Ocean Expedition Atlas, Vol. 7, Shorebased data and graphics. National Science Foundation, Washington, DC, 199 pp.

Ostlund, G. H. and C. Grall. 1988. Tritium Laboratory data report No 17.

Peng, T.-H., R. Wannikhof, J. L. Bullister, R. A. Feely and T. Takahashi. 1998. Quantification of decadal anthropogenic CO_2 uptake in the ocean based on dissolved inorganic carbon measurements. Nature, *396,* 560–563.

Polzin, K. L., J. M. Toole, J. R. Ledwell, R. W. Schmitz. 1997. Spatial variability of turbulent mixing in the abyssal ocean. Science, *276,* 93–96.

Reid, J. L. and R. J. Lynn. 1971. On the influence of the Norwegian-Greenland and Weddell Seas upon the bottom waters of the Indian and Pacific Oceans. Deep-Sea Res., *18,* 1063–1088.

Rhines, P. B. 1993. Oceanic General Circulation: Wave and Advection Dynamics, *in* Modeling Oceanic Climate Interactions, J. Willebrand and D. L. T. Anderson, eds., Springer-Verlag, 67–150.

Robbins, P. E. and J. M. Toole. 1997. The dissolved silica budget as a constraint on the meridional overturning circulation in the Indian Ocean. Deep-Sea Res., *44,* 879–906.

Stuiver, M. and H. G. Ostlund. 1983. GEOSECS Indian Ocean and Mediterranean radiocarbon. Radiocarbon, *25,* 1–20.

Stuiver, M., P. D. Quay and G. H. Ostlund. 1983. Abyssal water carbon-14 distribution and the age of the world oceans. Science, *219,* 849–851.

Talley, L. D. and M. O. Baringer. 1997. Preliminary results from WHP Sections 18N/15E in the Central Indian Ocean. Geophys. Res. Lett., *24*(21), 2789–2792.

Toole, J. M. and B. A. Warren. 1993. A hydrographic section across the subtropical South Indian Ocean. Deep Sea Res., I, *40,* 1973–2019.

U. S. World Ocean Circulation Experiment. 1993. U. S. contribution to the WOCE core project 1: The Program design for the Indian Ocean. U. S. WOCE. Exp. Off., College Station, Texas.

Veronis, G. 1981. Use of tracers in circulation studies, *in* The Sea, E. D. Goldberg, I. N. McCave, J. J. O'Brien, J. H. Steele, eds., Vol. 6, Ideas and Observations in the Study of the Seas, Wiley, NY 961 pp.

Warren, B. A. 1974. Deep flow in the Madgascar and Mascarene basins. Deep-Sea Res., *21,* 1–21, 1974.

—— 1977. Deep western boundary current in the eastern Indian Ocean. Science, *196,* 53–54.

—— 1981. Transindian hydrographic properties at Lat. 18°S: Property distributions and circulation in the South Indian Ocean. Deep-Sea Res., *28,* 759–788.

—— 1982. The deep water of the Central Indian Basin. J. Mar. Res. *40* (Suppl.), 823–860.

Weiss, R. F., W. S. Broecker, H. Craig and D. Spencer. 1983. GEOSECS Indian Ocean expedition atlas, Vol. 5, Hydrographic data 1977–1978. National Science Foundation, Washington, DC, 48 pp.

Whitworth, T., B. A. Warren, W. D. Nowlin, Jr., S. B. Rutz, R. D. Pillsbury and M. I. Moore. 1999. On the deep western-boundary current in the Southwest Pacific Basin. Prog. Oceanogr., *43,* 1–54.

You, Y. 1999. Dianeutral mixing, transformation and transport of the deep water of the Indian Ocean. Deep-Sea Res., I, *46,* 109–148.

Received: *16 March, 1999;* revised: *5 July, 2000.*